Adaptive Detection Algorithm for Hazardous Clouds Based on Infrared Remote Sensing Spectroscopy and the LASSO Method

Dacheng Li, Fangxiao Cui, Anjing Wang, Yangyu Li, Jun Wu, and Yanli Qiao

***Abstract*— Longwave infrared (LWIR) spectroscopy is useful for detecting and identifying hazardous clouds by passive remote sensing technology. Gaseous constituents are usually assumed to be thin plumes in a three-layer model, from which the spectral signatures are linearly superimposed on the brightness temperature spectrum. However, the thin-plume model performs poorly in cases of thick clouds. A modification to this method is made using synthetic references as target spectra, which allow linear models to be used for thick clouds. The prior background, which is generally unknown in most applications, is reconstructed through a regression method using predefined references. However, large residuals caused by fitting errors may distort the extracted spectral signatures and identification results if the predefined references are not consistent with the real spectral shapes. A group of references are generated to represent the possible spectral shapes, and the least absolute shrinkage and selection operator (LASSO) method is used to select the most appropriate reference for spectral fitting. Small residuals and adaptive identification are achieved by automatically selecting the reference spectrum. Two experiments are performed to verify the algorithm proposed in this article. Ethylene is adaptively detected during an indoor release process, and the spectral shape varies with the amount released. In addition, ammonia is measured under different humidity conditions, and the background is adaptively removed using the LASSO method. Based on this research, LWIR remote sensing technology can be applied in various target-detection scenarios, and adaptive identification is achieved to promote hazardous cloud detection.**

***Index Terms*— Brightness temperature spectrum, least absolute shrinkage and selection operator (LASSO), longwave infrared (LWIR), remote sensing.**

I. Introduction

REMOTE sensing is a powerful method for the detection of hazardous clouds allowing early warnings, which is important in many situations. Many techniques have been proposed to solve the identification problem of hazardous clouds, for example, infrared remote sensing [1], laser methods [2], and photoacoustic spectroscopy [3].

Among these remote sensing technologies, passive infrared remote sensing technology with longwave infrared (LWIR) spectroscopy is useful for identifying and classifying hazardous clouds. In out-field detection, most natural or anthropogenic objects are radiation sources that account for a major portion of the input energy measured by remote sensing instruments, and atmospheric constituents cause interference or clutter, hindering the classification of hazardous gases. The simplest way to deal with this interference is subtracting the measured background from the results or substituting neighborhood areas from the measured spectrum [4]–[6]. However, for most application scenarios, such as explosive gas confirmation or emergency support [7], [8], pure background information is usually difficult to obtain in advance, in which case the false alarm rate may increase because a background containing target information is subtracted and the detection rate may decrease if a background that is very different from the viewing background is subtracted. Some statistical detection algorithms have been proposed to overcome this problem. Multiple background objects can be measured simultaneously through hyperspectral imaging data, which enable the analysis of the distributed parameters of the background with statistical meaning [9]. By assuming a defined background distribution and regarding the gaseous plume as anomaly data represented by a heavy-tail distribution, the matched filter detector and adaptive coherent estimator can be applied in gas identification [1], [10]. These classification detectors are hindered by including the target gas pixels in statistical analyses without confirming the target and background pixels, and the detection rate is low due to atmospheric clutter information being retained in the spectra. Beil *et al.* [11] proposed a detection algorithm based on the brightness temperature (resolved in the spectrum) transformed from the radiance with the inverse function of Planck's radiation law. In the brightness temperature spectrum regime, the background objects are treated as baseline shifts because their signatures are generally slowly varying functions of the frequency, and all gas features are linearly superimposed on the baseline, which enables the reconstruction and removal of the background from the measured spectrum without background information [12]. The brightness temperature spectrum detection algorithm uses simulated references to obtain regression coefficients by fitting a single measured spectrum using the

Manuscript received August 27, 2019; revised January 1, 2020 and March 14, 2020; accepted April 19, 2020. This work was supported in part by the National Natural Science Foundation of China under Project 41505020, in part by the Laboratory Innovation Foundation of Chinese Academy of Sciences under Project CXJJ-19S002, and in part by the Key Deployment Project Foundation Chinese Academy of Sciences under Project KGFZD-135-16-002-2. *(Corresponding author: Fangxiao Cui.)*

Dacheng Li is with the Key Laboratory of Optical Calibration and Characterization, Anhui Institute of Optics and Fine Mechanics, Chinese Academy of Science, Hefei 230031, China, and also with the University of Science and Technology of China, Hefei 230026, China (e-mail: dcli@aiofm.ac.cn).

Fangxiao Cui, Anjing Wang, Yangyu Li, Jun Wu, and Yanli Qiao are with the Key Laboratory of Optical Calibration and Characterization, Anhui Institute of Optics and Fine Mechanics, Chinese Academy of Science, Hefei 230031, China (e-mail: fxcui@aiofm.ac.cn).

Color versions of one or more of the figures in this article are available online at http://ieeexplore.ieee.org.

Digital Object Identifier 10.1109/TGRS.2020.2989526

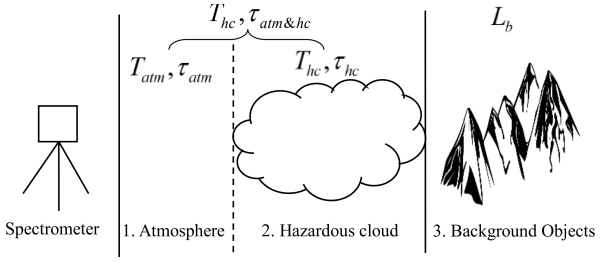

Fig. 1. Passive infrared remote sensing of hazardous clouds.

ordinary least squares (OLS) method. The background spectrum is reconstructed by the multiplication of background references and the corresponding regression coefficients, and the target signatures are extracted by subtracting the reconstructed background from the measured spectrum. This method works well in thin-plume cases and requires a simulated atmospheric spectrum similar to the measured conditions. However, this approach lacks adaptivity for the thick-cloud cases and different atmospheric conditions, for which improper references can lead to errors. A nonlinear optimal estimation procedure can be applied in the thick-cloud conditions, but it requires gas identification prior to implementation [13]. Thus, background removal and target identification are generally difficult to simultaneously accomplish from real-time measurements.

In recent machine-learning research, the least absolute shrinkage and selection operator (LASSO) method has been effectively advanced for data mining [14]. It has two main applications: feature selection and variable selection [15], [16]. Many band-selection algorithms have been proposed for hyperspectral image classification [17]–[19]. These algorithms use the "feature selection" function of LASSO to refine the model and obtain accurate classification results.

Here, we propose a detection algorithm for hazardous clouds based on the LASSO algorithm using its "variable selection" ability. If a group of references are simulated to indicate different cloud thicknesses, the most appropriate target reference can be chosen from the data set according to the measured spectrum. The same procedure applies to different atmospheric conditions. Through this "variable selection" procedure, we can obtain the most likely targets and atmospheric references from single measurements. The background is reconstructed with smaller residuals than those that result from the OLS method, and the target reference is approximately achieved for further qualitative and quantitative analyses. Through research on detection algorithms based on LASSO, LWIR remote sensing technology can be adaptively used for various target conditions and atmospheric environments, and better classification results are achieved by improving the feature-extraction process.

II. Detection Theory

A. Theory of LWIR Remote Sensing Technology

A vapor cloud is described by a simple three-layer model, as shown in Fig. 1. The first layer is the atmospheric layer, the second layer is the hazardous cloud, and the third layer is the background layer, which includes natural and anthropogenic objects. The distance between the spectrometer and the background objects is usually within several kilometers, and it is reasonable to assume that each layer is uniform and at same temperature. The hazardous cloud is dispersed through a wide range and fully fills the field of view of the spectrometer along the sight line. The radiance received by the spectrometer is the radiance propagated from the background objects through all layers, which is denoted by $L_{\text{meas}}(\upsilon)$ $(\text{W/m}^2 \cdot \text{Sr} \cdot \text{cm}^{-1})$

$$\begin{aligned} L_{\text{meas}}(\upsilon) = {} & (1-\tau_{\text{atm}}(\upsilon))B_{\text{atm}}(\text{T}_{\text{atm}}, \upsilon) \\ & + \tau_{\text{atm}}(\upsilon)[(1-\tau_{\text{hc}}(\upsilon))B_{\text{hc}}(\text{T}_{\text{hc}}, \upsilon) \\ & + \tau_{\text{hc}}(\upsilon)L_b(\upsilon)]. \end{aligned} \tag{1}$$

The subscript meas refers to the spectrum measured by the spectrometer, the subscript atm refers to the atmosphere, the subscript hc refers to the hazardous clouds, and the subscript b refers to the background objects. Hereinafter, all instances of these subscripts have the same meaning. τ is the transmittance of one layer, B is the blackbody radiance at temperature T, and L_b is the radiance of background objects before the plume. All parameters are resolved with wavenumber υ.

In an out-field scenario, the hazardous cloud is dispersed quickly and adequately mixed with the atmosphere, the first layer is at the same temperature as that of the second layer ($\text{T}_{\text{atm}} = \text{T}_{\text{hc}}$), and the radiance of the first two layers is equivalent ($B_{\text{atm}} = B_{\text{hc}}$). The transmittance of the first two layers can be combined into one layer by setting $\tau_{\text{atm\&hc}} = \tau_{\text{atm}}\tau_{\text{hc}}$. Upon substituting $\tau_{\text{atm\&hc}}$ into (1), the three-layer model can be simply written as follows:

$$L_{\text{meas}}(\upsilon) = (1-\tau_{\text{atm\&hc}}(\upsilon))B_{\text{hc}}(\text{T}_{\text{hc}}, \upsilon) + \tau_{\text{atm\&hc}}(\upsilon)L_b(\upsilon). \tag{2}$$

This equation can be expressed in ratio form as follows:

$$\tau_{\text{atm\&hc}}(\upsilon) = \frac{L_{\text{meas}}(\upsilon) - B_{\text{hc}}(\text{T}_{\text{hc}}, \upsilon)}{L_b(\upsilon) - B_{\text{hc}}(\text{T}_{\text{hc}}, \upsilon)}. \tag{3}$$

The radiance is transformed to the brightness temperature according to the inverse Planck's radiance law

$$\text{T}(\upsilon) = \frac{\text{hc}\upsilon}{k \ln\left[\frac{L(\upsilon)+2\text{hc}^2\upsilon^3}{L(\upsilon)}\right]} \tag{4}$$

where h is the Planck's constant, c is the speed of light, and k is the Boltzmann's constant.

In the brightness temperature spectrum, two constant temperatures are used to describe the background objects and the environment. By combining (4) and (3), we can obtain the following equation:

$$\begin{aligned} \tau_{\text{atm\&hc}}(\upsilon) &= \frac{\text{T}_{\text{meas}}(\upsilon) - \text{T}_{\text{hc}}}{\text{T}_b - \text{T}_{\text{hc}}} \\ &= e^{-\alpha(\upsilon)\text{CL}} \end{aligned} \tag{5}$$

where $\text{T}(\upsilon)$ is the brightness temperature spectrum, T_b is the temperature of the background objects, which are usually assumed to be blackbodies or gray bodies, $\alpha(\upsilon)$ is the absorption coefficient spectrum, and CL is the concentration

path length, which is the product of the concentration and path length.

The spectral signatures of the atmosphere and the signature of the vapor cloud appear on a constant baseline in the brightness temperature spectrum. Using $\Delta T = T_b - T_{hc}$ as the temperature difference between the background and the environment and $ST_{meas}(\upsilon) = T_b - T_{meas}(\upsilon)$ as the spectral signatures in the spectrum, (5) can be written as follows:

$$ST_{meas}(\upsilon) = \Delta T(1 - \tau_{atm\&hc}(\upsilon)). \tag{6}$$

In far-field detection, the total transmittance $\tau_{atm\&hc}$ is the product of the transmittance of the atmosphere and that of vapor clouds as follows:

$$\begin{aligned}\tau_{atm\&hc}(\upsilon) &= \tau_{atm}(\upsilon) \cdot \tau_{hc}(\upsilon) \\ &= e^{-[(\alpha(\upsilon)CL)|_{atm} + (\alpha(\upsilon)CL)|_{hc}]}.\end{aligned} \tag{7}$$

The features of hazardous clouds are extracted by subtraction of the atmospheric interference before identification. Since the multiplication form in (7) is hard to directly use for target extraction, a simple linear model is proposed to alleviate this problem.

B. Simple Linear Model and Target Feature Extraction by the OLS Method

If the target cloud is a single thin plume, the transmittance is approximately written as a linear combination of the atmosphere and the target cloud

$$\tau_{atm\&hc}(\upsilon) \approx 1 - (\alpha(\upsilon)|_{atm} \cdot CL|_{atm} + \alpha(\upsilon)|_{hc} \cdot CL|_{hc}). \tag{8}$$

By substituting (8) into (6), the spectral signatures can be written as follows:

$$\begin{aligned}ST_{meas}(\upsilon) \approx{}& \alpha(\upsilon)|_{atm} \cdot (CL|_{atm} \cdot \Delta T) \\ &+ \alpha(\upsilon)|_{hc} \cdot (CL|_{hc} \cdot \Delta T).\end{aligned} \tag{9}$$

From (9), the measured spectrum is approximately the linear summation of the atmosphere and the hazardous cloud. The absorbance spectrum $\alpha(\upsilon)$ can be obtained from the standard infrared database, which we call the reference spectrum, and the unknown parameters $(CL \cdot \Delta T)$ are evaluated by the OLS method. Then, target feature extraction is fulfilled by subtraction of the atmospheric part from the measured spectrum. The procedure is detailed in [12].

Using β as the corresponding coefficient $(CL \cdot \Delta T)$ of each signature, (9) is expressed in discrete form as follows:

$$ST_i = \sum_j \alpha_{ij}\beta_j. \tag{10}$$

The subscript i is the index of the wavenumber, and the subscript j is the index of the gas constituents, which here is regarded as the target vapor plume or atmosphere.

Equation (10) is written in matrix form as follows:

$$\mathbf{ST}_{meas} = \boldsymbol{\alpha}\boldsymbol{\beta} \tag{11}$$

where $\mathbf{ST}_{meas}$ is a column vector of length p, $\boldsymbol{\alpha}$ is the reference matrix of dimensions $p \times N$, where N is the number of gaseous constituents, and $\boldsymbol{\beta}$ is a column vector of length N, which is calculated by the OLS method as follows:

$$\boldsymbol{\beta} = \left(\boldsymbol{\alpha}^{\mathrm{T}}\boldsymbol{\alpha}\right)^{-1}\boldsymbol{\alpha}^{\mathrm{T}} \cdot \mathbf{ST}_{meas}. \tag{12}$$

Here, the superscript $^{\mathrm{T}}$ is the transposition of the vector, and this notation is the same and omitted from explanation in Section III.

The measured spectrum usually has a slowly varying baseline shift due to thermal effects inside the spectrometer. Thus, the reference matrix $\boldsymbol{\alpha}$ has threefold reference data. The first is the spectral signature of the target plume, which is written as $\boldsymbol{\alpha}_{hc}$, the second is the spectral signature of the atmosphere, which is written as $\boldsymbol{\alpha}_{atm}$, and the third is the baseline fitting function, which is written as $\boldsymbol{\alpha}_{bs}$ and is generated by slowly varying wide Gaussian functions. The corresponding coefficients of each part are $\boldsymbol{\beta}_{hc}$, $\boldsymbol{\beta}_{atm}$, and $\boldsymbol{\beta}_{bs}$, respectively. The target feature is extracted by subtraction fitting of the atmosphere and baseline

$$\mathbf{ST}_{hc} = \mathbf{ST}_{meas} - \left(\boldsymbol{\alpha}_{atm}\boldsymbol{\beta}_{hc} + \boldsymbol{\alpha}_{bs}\boldsymbol{\beta}_{bs}\right) \tag{13}$$

where $\mathbf{ST}_{hc}$ is the extracted target feature in discrete form with length p.

C. Modification for the Brightness Temperature Spectrum Theory

The brightness temperature spectrum theory is based on the assumption that all gaseous constituents in the optical path are thin plumes, and from (8), the total transmittance is expressed by a linear combination of the spectral signatures of all plumes. With the known spectral signatures of the target plume and atmosphere, the measured brightness temperature spectrum is fit, and the background is reconstructed through a regression method.

However, in many application scenarios, the assumption of a thin plume is unreasonable and results in a low detection rate; moreover, constant-atmosphere references are not adapted based on various atmospheric conditions, such as humidity. A nonlinear iteration method may solve adaptivity issues under various atmospheric conditions but requires identification of the initial target plume [13], and there is often a low detection rate due to the nonremoval of the background.

To solve the transmittance product problem in (7) and use a linear model for the thick-cloud case, we modify the approach considering the brightness temperature spectrum theory. In the thin-plume case (usually, $\alpha CL \leq 0.1$), the spectral shape of the transmittance is very close to that of the absorption coefficient [11]. We assume that the synthetic transmittance $\tau^*_{atm\&hc}(\upsilon)$ has the same spectral shape as that of the transmittance of a thick cloud but in a scaled form of the value of $\tau_{atm\&hc}(\upsilon)$

$$\left(1 - \tau^*_{atm\&hc}(\upsilon)\right) = \varepsilon(1 - \tau_{atm\&hc}(\upsilon)) \tag{14}$$

where ε is the scale factor. The wavenumber υ is also omitted in the following paragraph.

If a thick cloud is defined as $0 \leq \tau_{atm\&hc} \leq 0.9$ and we define a synthetic thin cloud as $\tau^* = 0.9$, the scale factor ranges from $1 \leq \varepsilon \leq 10$. Given synthetic spectral

signatures α^*_{atm} and α^*_{hc}, τ^*_{atm} and τ^*_{hc} are approximately expressed in linear form, respectively,

$$\begin{cases} (1-\tau^*_{\text{atm}}) \approx \alpha^*_{\text{atm}}\beta^*_{\text{atm}} \\ (1-\tau^*_{\text{hc}}) \approx \alpha^*_{\text{hc}}\beta^*_{\text{hc}}. \end{cases} \tag{15}$$

Here, β^*_{atm} and β^*_{hc} are the coefficients similar to the CL value respective of the atmosphere and the hazardous cloud.

From (7), (14), and (15), the total transmittance of thick clouds is written as follows:

$$\begin{aligned} (1-\tau_{\text{atm\&hc}}) &= (1-\tau_{\text{atm}}\tau_{\text{hc}}) \\ &= 1-\left[1-\frac{1}{\varepsilon_{\text{atm}}}(1-\tau^*_{\text{atm}})\right]\left[1-\frac{1}{\varepsilon_{\text{hc}}}(1-\tau^*_{\text{hc}})\right] \\ &\approx \frac{\alpha^*_{\text{atm}}\beta^*_{\text{atm}}}{\varepsilon_{\text{atm}}}+\frac{\alpha^*_{\text{hc}}\beta^*_{\text{hc}}}{\varepsilon_{\text{hc}}}-\frac{\alpha^*_{\text{atm}}\beta^*_{\text{atm}}}{\varepsilon_{\text{atm}}}\cdot\frac{\alpha^*_{\text{hc}}\beta^*_{\text{hc}}}{\varepsilon_{\text{hc}}} \\ &\approx \alpha^*_{\text{atm}}\frac{\beta^*_{\text{atm}}}{\varepsilon_{\text{atm}}}+\alpha^*_{\text{hc}}\frac{\beta^*_{\text{hc}}}{\varepsilon_{\text{hc}}}. \end{aligned} \tag{16}$$

Since $1 \le \varepsilon_{\text{atm}} + \varepsilon_{\text{hc}} \le 10$, $\tau^*_{\text{atm}} = 0.9$, and $\tau^*_{\text{hc}} = 0.9$, the third part on the third line of (16) is far smaller than the other parts and can be omitted in linear approximation. From (6) and (16), the spectral signatures in the brightness temperature spectrum of (9) are written as a linear combination of the synthetic signatures for thick clouds as follows:

$$\text{ST}_{\text{meas}} \approx \alpha^*_{\text{atm}} \cdot \left(\beta^*_{\text{atm}} \cdot \Delta\text{T}\right) + \alpha^*_{\text{hc}} \cdot \left(\beta^*_{\text{hc}} \cdot \Delta\text{T}\right). \tag{17}$$

In this case, the linear model of (11) still holds. The synthetic spectral signature α^* is dependent on CL, and the most natural approach is to assume that this value is based on a linear transformation of the transmittance

$$\alpha^*(\upsilon, \text{CL}) = \text{A}\left(1-e^{-\alpha(\upsilon)\text{CL}}\right) \tag{18}$$

where A is a scaled factor that can be combined with coefficient β; therefore, the transmittance spectrum is henceforth directly used to obtain α^*. Here, the subscripts atm and hc in α^* are not shown, and equation (18) has the same form for every gaseous constituent.

A simulation experiment is performed to show the modification of the brightness temperature spectrum theory. The brightness temperature spectrum of methanol is simulated in the 700–1400 cm^{-1} range at a resolution of 4 cm^{-1}, as shown in Fig. 2. The atmosphere reference is calculated using MODTRAN. The reference of methanol is used according to the absorption coefficient spectrum for a simple linear model, and the synthetic reference is used for the modified theory, as shown in Fig. 3.

This simulation ignores the baseline shifting effect. Using methanol and the atmosphere as references, the measured spectrum is fitted by the OLS method. The simple linear model uses the absorption coefficient spectrum as the methanol reference, whereas the modified model uses the synthetic reference as the methanol reference, and the fitting results are shown in Fig. 4. Large residuals are left from using the absorption coefficient as the methanol absorption coefficient reference, but small residuals are achieved using the synthetic reference.

Therefore, the chosen references have a considerable effect on the fitting procedure. Through the modification of the

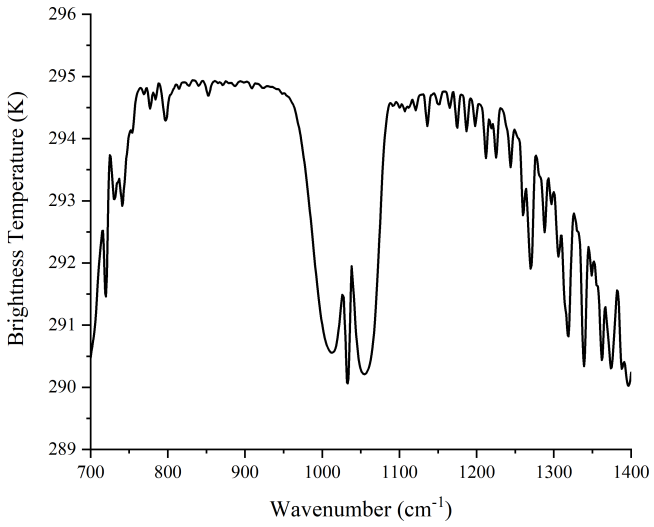

Fig. 2. Simulated brightness temperature spectrum of thick-cloud methanol.

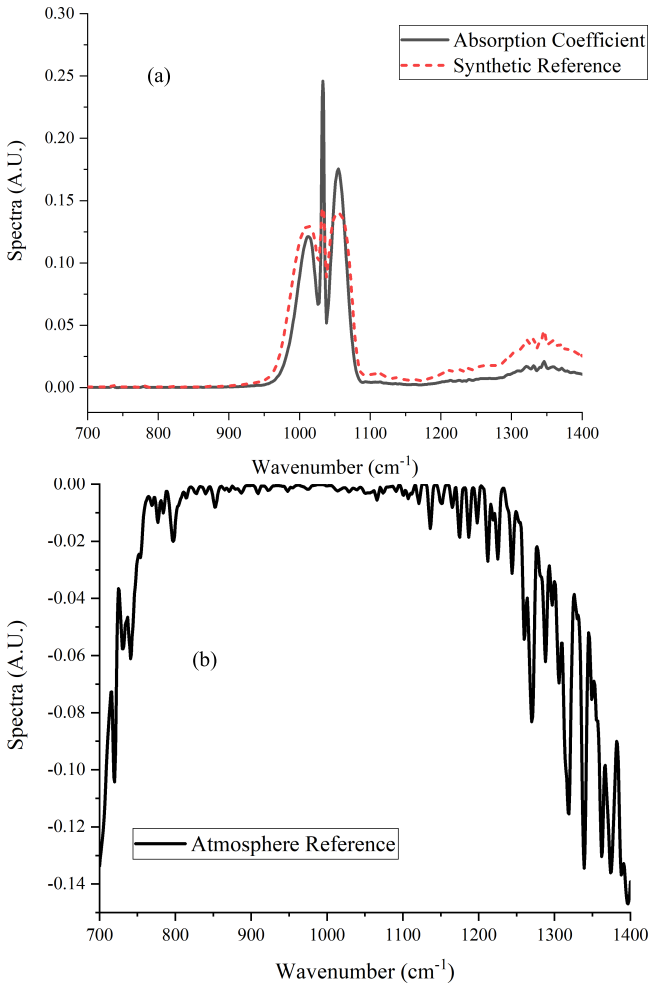

Fig. 3. Reference spectra of methanol and atmosphere. (a) Reference spectrum of methanol, where the solid line is the absorption coefficient and the dashed line is the synthetic reference. (b) Reference spectrum for atmosphere. All spectra are normalized for clarity.

brightness temperature spectrum theory, the linear model still works for the thick-cloud cases. However, in real applications, the exact CL value is unknown, and the synthetic reference

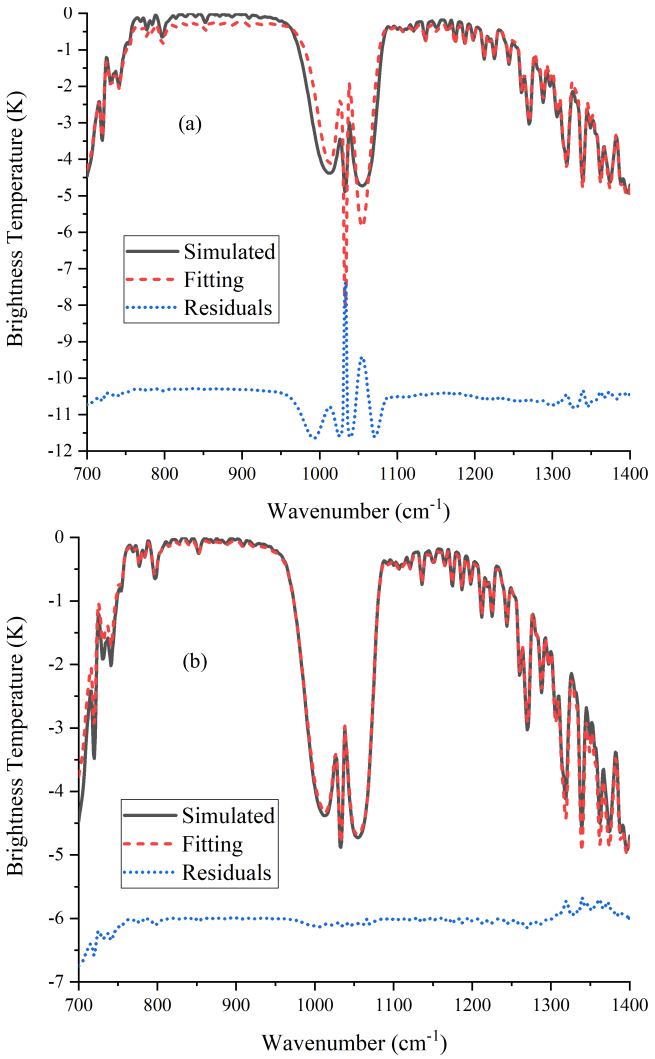

Fig. 4. Fitting results achieved using different references, with residuals from the subtraction of the simulated and fit values. (a) Fitting results using the absorption coefficient reference for methanol. (b) Fitting results using the synthetic reference for methanol. All spectra are normalized and shifted for clear display.

cannot be created without prior information. Thus, a group of references are generated for several typical CL values for one plume to cover most possible cases, and the best approximation is chosen according to the measured data. In this way, adaptive detection can be performed for thick clouds. The LASSO method is suited for this problem due to its "variable selection" merit.

III. Feature-Extraction Algorithm Based on the LASSO Method

A. LASSO Method

The LASSO method was first introduced in [20] and formulated by Tibshirani [21]. It is a powerful method that performs two main tasks: regularization and variable selection. The traditional OLS method may conduct unbiased estimation, but it usually has a large variance in the case of too many variables. In addition, it cannot handle collinear data. The LASSO method is a biased estimation method that involves some regularization of the optimized function. The regularization is in the L1 form in that the sum of the absolute values of the regression coefficients is forced to be less than a fixed value. It performs variable shrinkage by setting the corresponding regression coefficients to 0, and a refined model is achieved.

We will refer to the formulation used in [22]. Considering N sample data $\mathbf{X}$ with dimensions p by N, where the ith sample is $X_i := (x_{1i}, x_{2i}, \ldots, x_{pi})^{\mathrm{T}}$, then the outcome vector is $\mathbf{Y}$ with dimensions p by 1. By letting $\beta = (\beta_1, \beta_2, \ldots, \beta_N)$, the LASSO estimate is defined by the solution to the L1 optimization problem

$$\min \left(\frac{1}{p} \sum_{i=1}^{p} \left(Y_i - \sum_{j=1}^{N} x_{ij} \beta_j \right)^2 \right) \text{ subject to } \sum_{j=1}^{N} |\beta_j| \le t. \tag{19}$$

Here, $t \ge 0$ is a prespecified free parameter that determines the upper bound of regularization.

This optimization problem is equivalent to parameter estimation as follows:

$$\widehat{\beta}(\lambda) = \arg\min_{\beta} \left(\frac{1}{p} \sum_{i=1}^{p} \left(Y_i - \sum_{j=1}^{N} x_{ij} \beta_j \right)^2 + \lambda \sum_{j=1}^{N} |\beta_j| \right). \tag{20}$$

Here, $\lambda \ge 0$ is the parameter that controls the strength of the penalty. The relationship between λ and t is a reverse relationship. λ becomes 0 as t becomes infinity, and the problem becomes an OLS problem.

B. Variable Selection via LASSO

When we minimize the optimization problem, some coefficients decrease to 0, for example, $\beta_j(\lambda) = 0$ for some values of j (depending on the value of λ). Therefore, variables with a coefficient equal to 0 are excluded from the model.

As mentioned in Section II, the dilemma of spectral feature extraction lies in that the measured spectrum fitting requires the exact spectral line shape of every gas constituent, which is related to the CL value, while the presence of the target gas is unknown, in addition to the CL value.

Unlike the use of one fixed reference spectrum for one gas constituent in Section II-B, a group of reference spectra are generated for one gas constituent to represent possible thicknesses of the cloud cases, and the most correlated spectrum for each group is selected via the LASSO method. Therefore, a group of reference spectra must be set up before measurement.

C. Reference Spectra Preparation

Here, we consider only one target cloud case, and the interference constituents are ordinary gases of the atmosphere. More complicated cases, such as those involving multiple target clouds and the presence of unusual interferences, could be dealt with in the same way.

Before reference spectra preparation, the similarity standard of every spectrum in one group must be designated.

Here, we use a correlation coefficient f_{cc} to measure the similarity, and it is written as follows:

$$f_{\text{cc}} = \frac{(\mathbf{x_1}-\bar{\mathbf{x}}_\mathbf{1})^{\text{T}}(\mathbf{x_2}-\bar{\mathbf{x}}_\mathbf{2})}{\|\mathbf{x_1}-\bar{\mathbf{x}}_\mathbf{1}\| \cdot \|\mathbf{x_2}-\bar{\mathbf{x}}_\mathbf{2}\|} \tag{21}$$

where $\mathbf{x}$ is a column vector of length N with the subscript $i = 1, 2$ representing two spectra; $\bar{\mathbf{x}}$ is the mean value of vector $\mathbf{x}$; and $\|\|$ is the norm of the vector.

The value of f_{cc} is between 0 and 1, and the two spectra are more similar when f_{cc} approaches 1. In the following sections, (21) is also used in the identification of the extracted features by setting a threshold. The measured spectrum is identified as the target if f_{cc} exceeds the threshold.

In far-field remote sensing scenarios, the hazardous clouds often have finite CL values if they can be detected. It is impossible to simulate all cases of cloud thickness, but a few typical target references can be used to represent all thicknesses within an error tolerance range. This is similar to the use of center data to represent a cluster within a data set, with one spectrum used to represent a group of spectra within a similar area. Here, we use f_{cc} to calculate the similarity of spectra in one group, and a threshold is designated as the lower bound to indicate the similarity within the cluster, for example, 0.99.

The atmosphere provides permanent interference including that from water vapor, carbon dioxide, ozone, and other trace gases. Given specific parameters, the spectrum of the atmosphere is computed by a radiative transfer model such as MODTRAN. However, in real application scenarios, the humidity and optical length usually vary unpredictably, and a reasonable method for use involves simulating all possible spectra for different atmospheric conditions and selecting an approximation to remove atmospheric clutter. A group of typical atmosphere spectra are generated to represent all possible atmospheric conditions within an error range in the same way.

All references are aggregated for each group, from which the best approximation is selected, and small residuals are obtained by exactly fitting the measured spectrum. In addition, the background is adaptively removed from the measured spectrum. By selecting the spectral signatures of the target plume, an accurate identification result is achieved, even if no prior information for the target is available.

D. Feature-Extraction Algorithm Based on LASSO

A detection algorithm using the LASSO method is described here. The reference matrix is $\mathbf{X}_{p\times N}$, with the spectral dimension of p and the number of reference spectra of N. The N references are divided into three classes. The numbers of target and atmospheric references are N_{hc} and N_{atm}, respectively. The remaining $N - N_{\text{hc}} - N_{\text{atm}}$ references are baseline fitting functions, which are written as N_{bs}. The measured spectrum is $\mathbf{Y}_{p\times 1}$ for the brightness temperature.

The alternating direction method of multipliers (ADMMs) algorithm is used to solve the LASSO problem [23]. This procedure is iterated with λ decreasing from $\lambda_{\max}$ to $\lambda_{\min}$. $\lambda_{\min}$ is a small value, for example, $10^{-4} \cdot \lambda_{\max}$, and $\lambda_{\max}$ is the stopping criterion, which we used as proposed by Boyd *et al*. [23] as follows:

$$\lambda_{\max} = \|\mathbf{X}^{\text{T}}\mathbf{Y}\|_\infty. \tag{22}$$

An iteration number m is set to determine the iteration steps, with $\lambda_{\text{step}} = (\lambda_{\max} - \lambda_{\min})/m$, and for the ith step, $\lambda_i = \lambda_{\max} - i \cdot \lambda_{\text{step}}$.

When the iteration process is completed, the reference of the first nonzero coefficient is used as the selection for the target and the atmosphere, respectively.

By combining the selected target and atmosphere references as well as the original baseline fitting functions, a new reference matrix is generated to fit the measured spectrum via the OLS method, as in Section II-B. The background is reconstructed and removed to extract the target signature using this new reference matrix. In the identification step, the selected target reference is used as the standard target reference, but the simple linear model uses the absorption coefficient spectrum as the standard target reference, which may produce low correlation results and lower the detection rate.

The algorithm procedure is as follows (see Fig. 5).

1) Simulate all synthetic references by (18) from thin-plume to saturated-cloud conditions, and choose a central reference spectrum to represent a cluster of spectra that have a correlation coefficient with the central reference spectrum of above 0.99. Use the generated N_{hc} target gas references to construct the target reference matrix.
2) Use MODTRAN to simulate the atmospheric spectra under different humidity conditions and optical path lengths. Select N_{atm} typical references to construct the atmosphere reference matrix, as in step 1).
3) Use wide Gaussian functions to fit the baseline. Combine the target, atmosphere, and baseline into reference matrix $\mathbf{X}_{p\times N}$.
4) Transform the measured spectrum into the brightness temperature $\mathbf{Y}$.
5) Normalize $\mathbf{Y}$ and each column of $\mathbf{X}$.
6) Use the ADMM algorithm to solve the LASSO problem to obtain the regression coefficient $\boldsymbol{\beta}$.
7) Choose the reference corresponding to the first nonzero coefficient in $\boldsymbol{\beta}_{\text{hc}}$ as the target reference. If there are multiple nonzero coefficients, then choose the one with biggest absolute value as the target reference. The atmospheric reference is selected in the same way as the target reference.
8) Use the selected target reference, selected atmospheric reference, and original baseline functions to construct the new reference matrix $\mathbf{X}_{\text{new}}$, and compute the regression coefficient $\boldsymbol{\beta}_{\text{new}}$ by the OLS method.
9) Reconstruct the background spectrum using the atmosphere and baseline references in $\mathbf{X}_{\text{new}}$, and extract the target signatures after subtracting the reconstructed background from the measured spectrum.
10) Use the target reference selected in step 7) as the standard target reference, and calculate correlation coefficient f_{cc} of the extracted target signatures with the standard reference. The target is identified by comparison

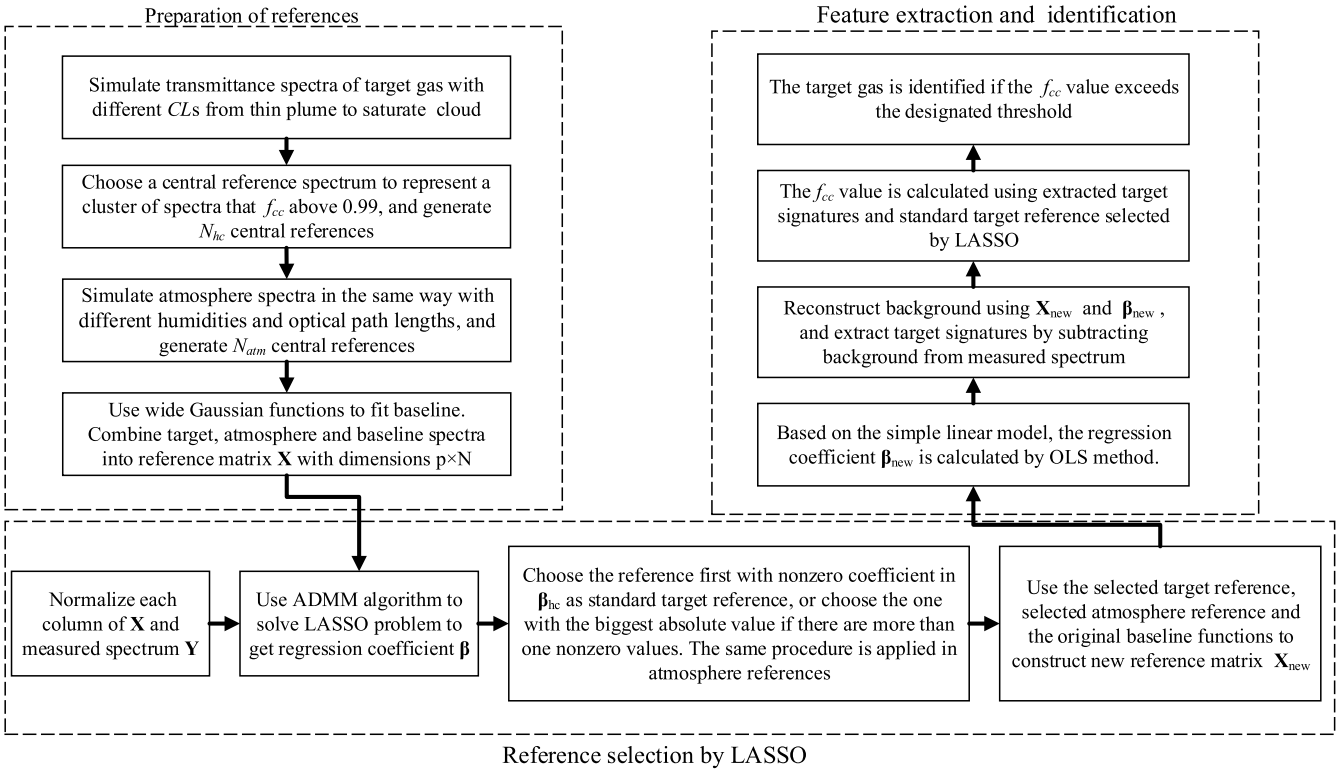

Fig. 5. Flowchart of the algorithm.

TABLE I
PARAMETERS OF THE EXPERIMENTAL INSTRUMENT

Name	Specifications
Spectral resolution (cm^{-1})	4
Working spectral range (cm^{-1})	700-1400
Detector type	Stirling MCT Detector
Noise equivalent temperature (mK)	80
Detection distance (km)	3-5
View angle (mrad)	30

with the predefined threshold. The threshold can be set to different values for different target gases.

IV. EXPERIMENTS AND DISCUSSION

Two experiments are performed to verify the validity of the algorithm proposed in this article. One experiment involves an indoor ethylene release at different concentrations to validate the target identification without a known prespecified plume concentration. The other experiment involves far-field ammonia detection at different humidity levels to validate the target detection method for various atmospheric conditions.

Two methods are compared using the experimental data. One is the LASSO method based on the modified brightness temperature model, which we refer to as LASSO in the following section. The other is a method proposed by Harig and Matz [12] based on a simple linear model, which uses the absorption spectrum as the target reference, and we refer to this method as OLS in the following section.

A Bruker OPAG33 FTIR spectrometer is used in the experiments, as shown in Fig. 6. The instrumental parameters are listed in Table I. The video camera is used for image acquisition to locate the release point. The spectrometer is fixed on a tripod and used to measure the spectra within the field of view. All gaseous constituents are detected in the spectral range of 700–1400 cm^{-1} at a resolution of 4 cm^{-1}.

A. Indoor Ethylene Release Detection

Ethylene is used in many industrial applications. It has a wide spectral feature within the 850–1080 cm^{-1} band and a narrow spectral feature in the 900–1000 cm^{-1} band. Its spectral shape becomes fat in the case of thick clouds. Ethylene from an indoor release is detected at close distances, with different spectral shapes in the release process (see Fig. 7).

Since indoor detection occurs at a very close distance, the atmospheric components are omitted in reference preparation. The reference spectra, including those of ethylene and the baseline functions, are considered for this experiment.

In this article, we use $\tau_{hc} = 0.99$ for the thin-plume case and $\tau_{hc} = 0$ for saturated clouds, and the transmittance value τ_{hc} is calculated using the maximal absorption coefficient. The transmittance spectra of ethylene are simulated for different CLs ranging from a very thin plume to a very thick cloud. A spectrum is used to represent a cluster of spectra with f_{cc} above 0.99, and four spectra are generated to represent different CL cases, as shown in Fig. 8(a). The OLS method uses the absorption coefficient spectrum as the target reference, as shown in Fig. 8(b). The baseline fitting uses wide Gaussian functions, which are uniformly distant at 200 cm^{-1}, with a full-width at half-maximum of 300 cm^{-1}.

First, the measured spectra in Fig. 7 are normalized. The ADMM algorithm is used to solve the LASSO problem by

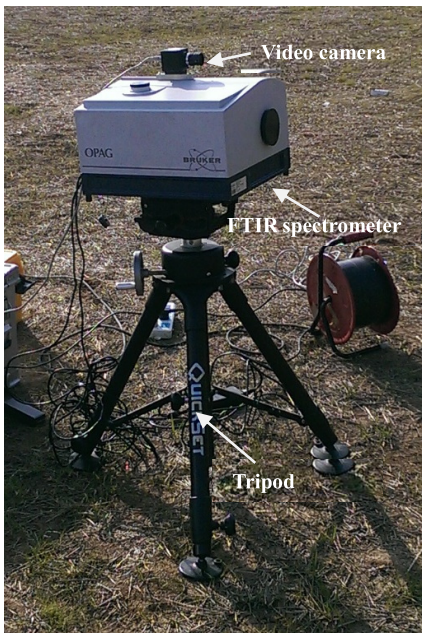

Fig. 6. Bruker OPAG33 FTIR spectrometer.

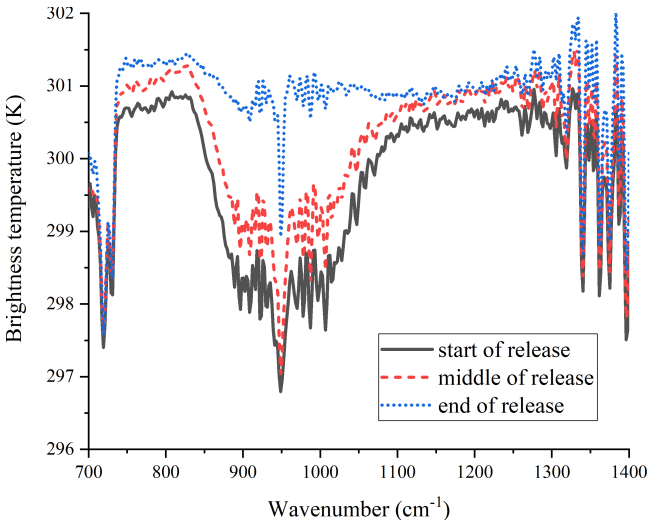

Fig. 7. Ethylene brightness temperature spectra from an indoor release process.

setting the number of iterations to 50. The regression coefficients with the corresponding iteration numbers are shown in the trace plots, from which the first nonzero values are selected as indices for the ethylene references.

The LASSO regression for the start of the release case is shown in Fig. 9. Index 4 is selected in the first iteration, which corresponds to the fourth reference in Fig. 8(a).

A new reference matrix is generated by combining the fourth reference in Fig. 8(a) and the original baseline fitting functions, and the measured spectrum is fitted using this new reference matrix. The OLS method uses the target reference in Fig. 8(b) and the same baseline fitting functions. A comparison of these two methods is shown in Fig. 10 for the start of the release case. The residuals from the LASSO method are smaller than those from the OLS method, especially for

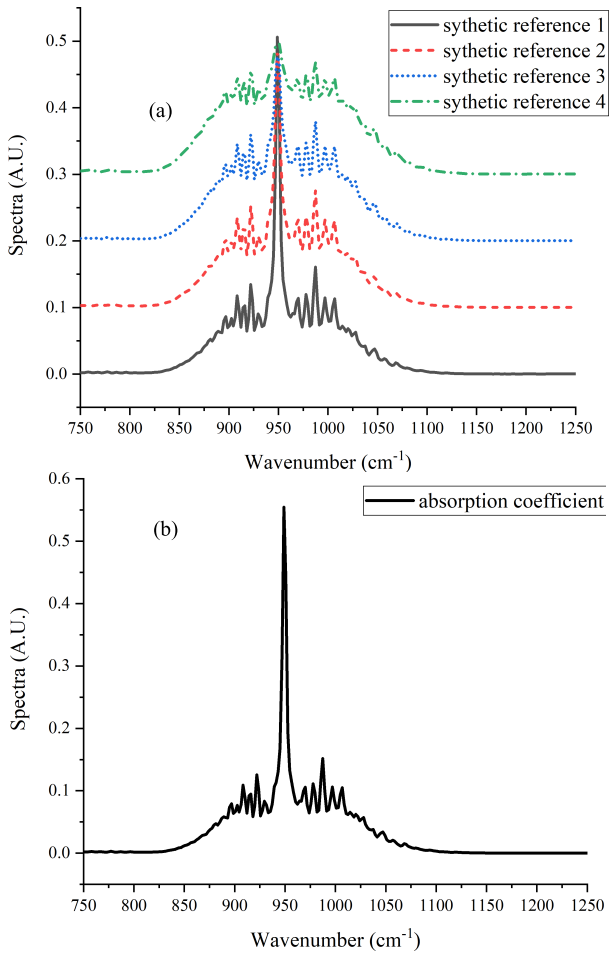

Fig. 8. Ethylene references used for fitting, with all spectra normalized and shifted for clarity. (a) Four synthetic spectra generated for LASSO. (b) Absorption coefficient spectrum for OLS.

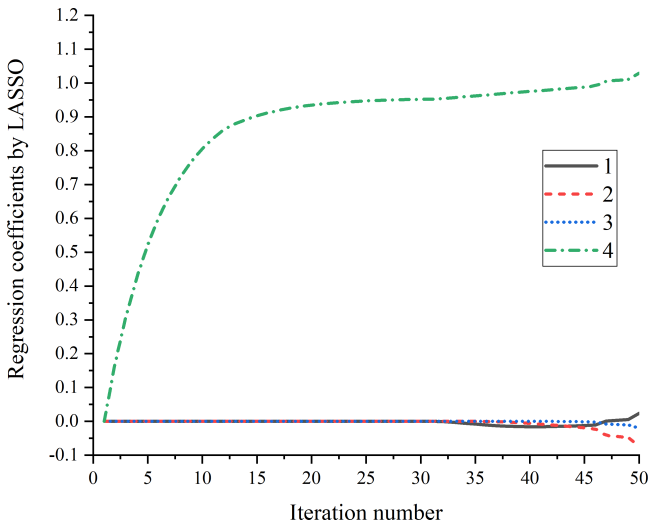

Fig. 9. Regression coefficients of the LASSO method plotted versus the iteration number for the start of the release case.

the weak absorption features in the 900–1000 cm^{-1} band. The weak absorption features become more prominent relative to the strong absorption feature at 950 cm^{-1} with an increase in the CL value. The OLS method uses a reference spectrum to

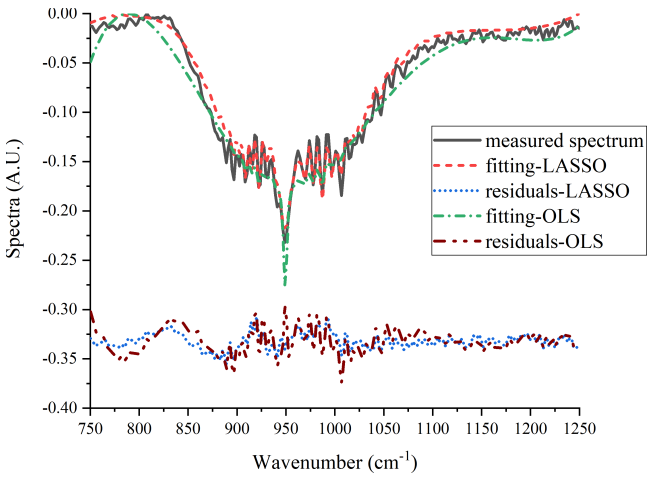

Fig. 10. Comparison of the LASSO method and the OLS method in fitting for the start of the release case. All spectra are normalized and shifted for clarity. The fitting LASSO uses the fifth reference in Fig. 8(a) as the target reference, and the OLS method uses the target reference in Fig. 8(b). The residuals are subtraction-fitted from the measured spectrum.

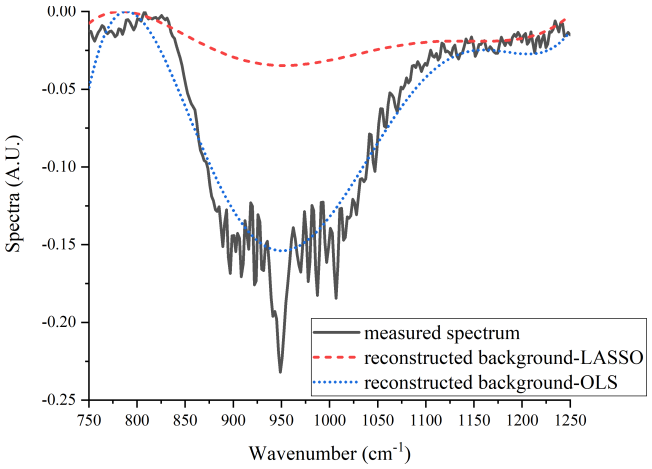

Fig. 11. Comparison of the backgrounds reconstructed by the two methods. All spectra are normalized and shifted for clarity.

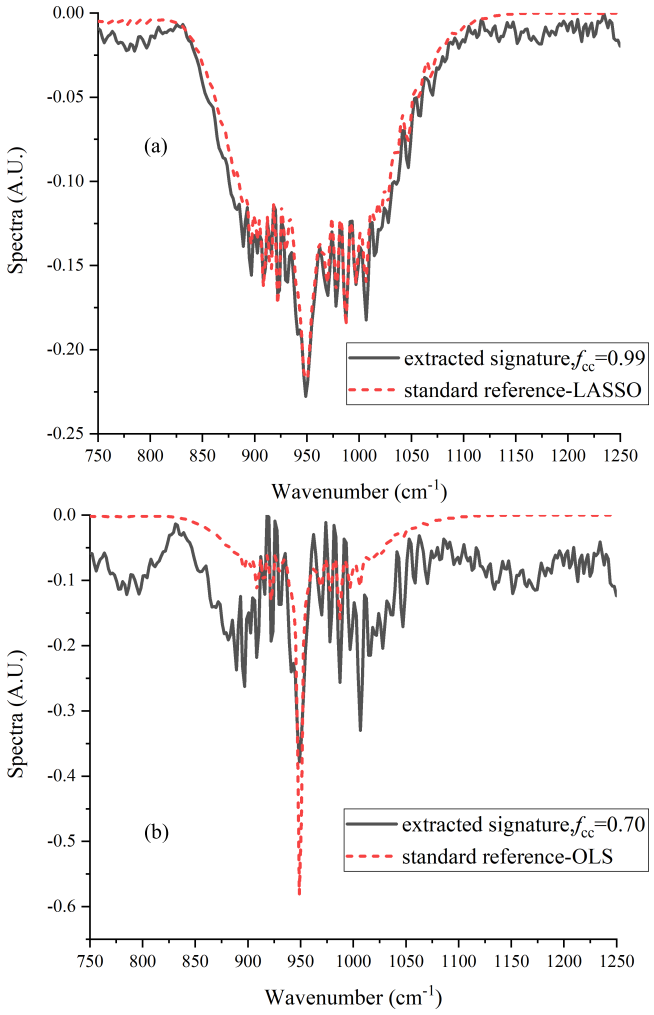

Fig. 12. Comparison of the extracted signatures and identification results for the LASSO and OLS methods for the start of the release case. All spectra are normalized and shifted for clarity. (a) Extracted signature and standard reference from the LASSO method, with $f_{cc} = 0.99$. (b) Extracted signature and standard reference from the OLS method, with $f_{cc} = 0.70$.

represent the thin-plume case, which mistakenly fits the broad feature as the baseline and excessively omits weak features. The LASSO method properly figures out the reference spectrum for the thick-cloud case, which conforms to the reality and achieves better fitting results.

Here, the reconstructed background uses only the baseline fitting functions because of omission of the atmosphere. The reconstructed background is shown in Fig. 11, from which we can see that the background reconstructed by the LASSO method is a wide baseline, whereas the OLS method misrecognizes the wide spectral feature of ethylene as the background.

The spectral signature is extracted by subtraction of the reconstructed background from the measured spectrum. The f_{cc} value of the extracted feature and the target standard reference is used for simple identification. The standard reference is the selected reference for the LASSO method, whereas that for the OLS method is the absorption coefficient spectrum. The comparison of the results is shown in Fig. 12. The signature extracted by the LASSO method retains most of the information of the measured spectrum, whereas the OLS method loses some useful information. The standard reference selected by LASSO is more suitable for identification, for which the f_{cc} value of 0.99 is far better than that of the OLS method.

A fixed threshold is used for identification, for example, 0.80, and then, Fig. 12(a) is identified as ethylene, while Fig. 12(b) is not. We will not discuss the identification method further, but apparently the LASSO method has a better detection rate.

The spectrum of ethylene in the middle release case is slightly different from that in the start release case. The spectral feature of the 950 cm^{-1} band becomes slightly deeper.

The LASSO regression is shown in Fig. 13. The fourth reference is selected as the target reference, but the third is very close to the fourth in the regression trace plot.

A new reference matrix is generated in combination with the fourth reference in Fig. 8(a), similar to the process used for the start of the release case. A comparison of these two methods is shown in Fig. 14. The residuals for the LASSO method are smaller than those for the OLS method, but the spectral peak loses full consistency at 950 cm^{-1}.

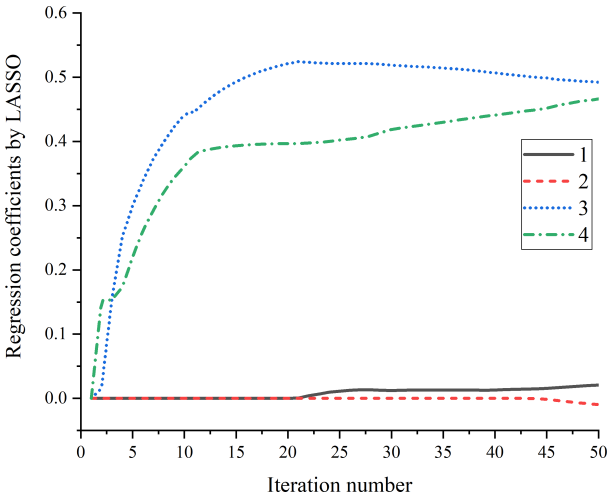

Fig. 13. Regression coefficients of the LASSO method plotted versus t.

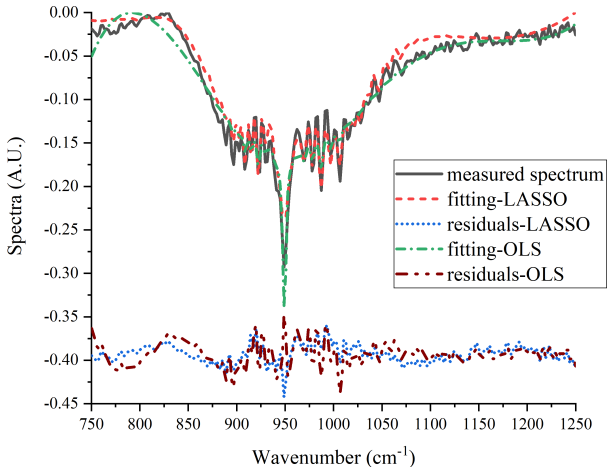

Fig. 14. Comparison of the LASSO method and the OLS method in fitting for the middle release case. All spectra are normalized and shifted for clarity. The LASSO fitting uses the fourth reference in Fig. 8(a) as the target reference, and the OLS method uses the target reference in Fig. 8(b). The residuals are subtraction-fitted from the measured spectrum.

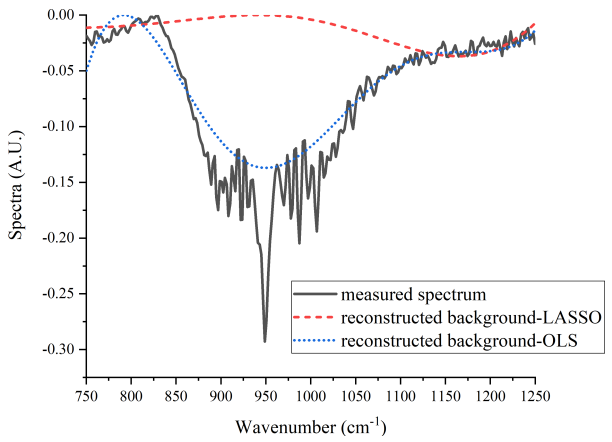

Fig. 15. Comparison of the reconstructed backgrounds from the two methods. All spectra are normalized and shifted for clarity.

The comparison of the reconstructed background is shown in Fig. 15. We can see that the OLS method misrecognizes the wide spectral feature of ethylene as the background, whereas the LASSO method does well in background evaluation.

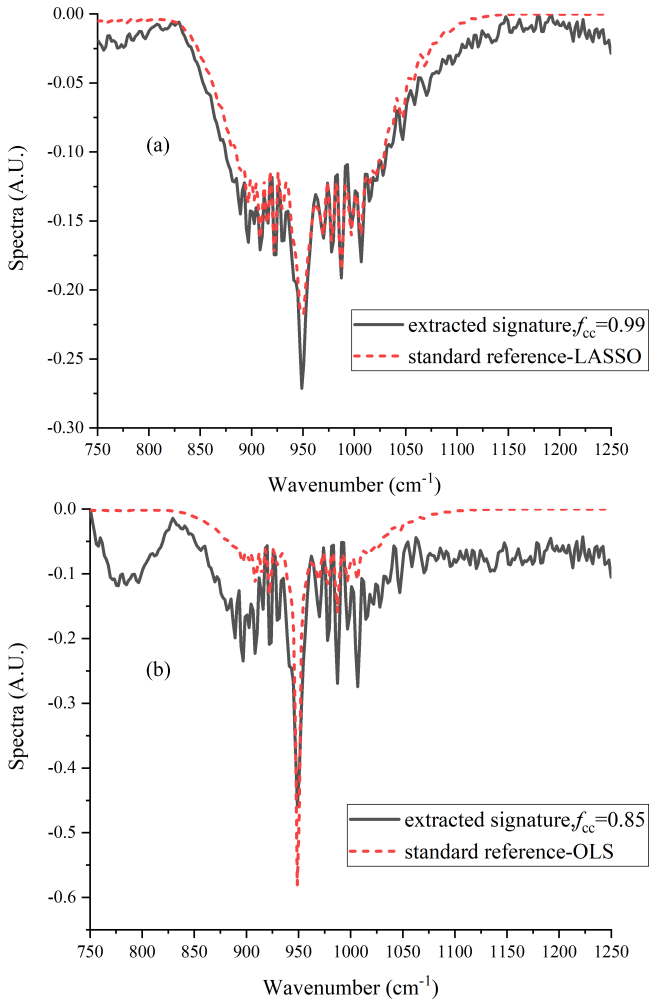

Fig. 16. Comparison of the extracted signatures and identification results for the LASSO and OLS methods for the middle release case. All spectra are normalized and shifted for clarity. (a) Extracted signature and standard reference from the LASSO method, with $f_{cc} = 0.99$. (b) Extracted signature and standard reference from the OLS method, with $f_{cc} = 0.85$.

The extracted signatures and identifications are shown in Fig. 16. The f_{cc} value of 0.99 for LASSO is better than that for the OLS method. Because the spectral features become narrower in the 950 cm^{-1} band, the detection result improves for the OLS method for the start of the release case. However, the LASSO method still performs well in these two cases.

At the end of release, the ethylene cloud becomes a thin plume, and the spectral features of the 850–1080 cm^{-1} band become narrow.

The LASSO regression is shown in Fig. 17. The first reference is selected as the target reference in the first place.

A new reference matrix is generated by combining the first reference in Fig. 8(a), similar to the process for the start of the release case. A comparison of these two methods is shown in Fig. 18. The fitting results and the residuals are almost the same for these two methods.

The extracted signature and identification are shown in Fig. 19. The f_{cc} values are almost the same, and the identification performs the same for these two methods.

From the ethylene release experiment, we can find that the OLS method is only suitable for the thin-plume case, but the

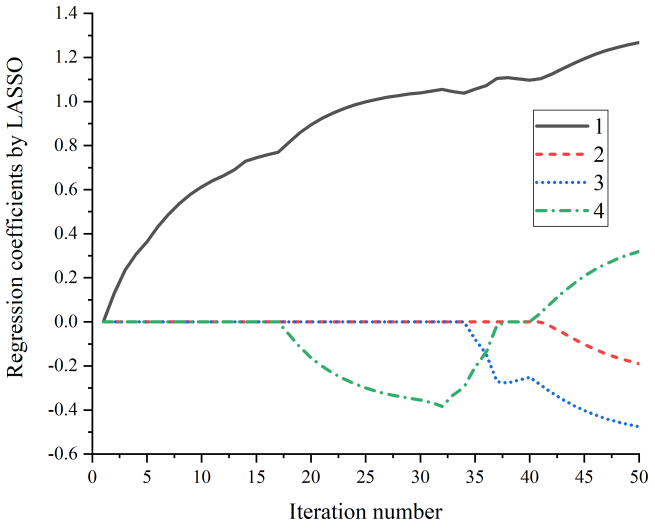

Fig. 17. Regression coefficients of the LASSO method plotted versus the iteration number for the end release case. The iteration number for the middle release case.

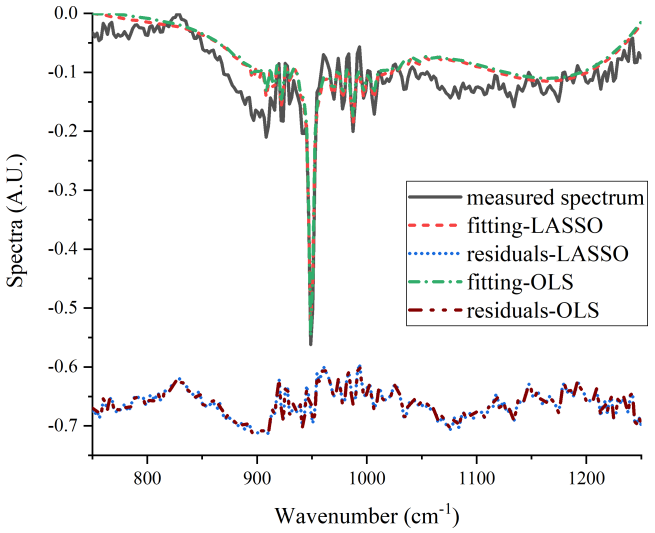

Fig. 18. Comparison of the LASSO method and the OLS method in fitting for the end of the release case. All spectra are normalized and shifted for clarity. The LASSO fitting uses the first reference in Fig. 8(a) as the target reference, and the OLS method uses the target reference in Fig. 8(b). The residuals are subtraction-fitted from the measured spectrum.

LASSO method performs well and consistently in different thick-cloud cases. The background is adaptively reconstructed and removed. In addition, by selecting the appropriate standard reference for identification, better classification results are achieved.

B. Ammonia Detection Under Different Humidity Conditions

In many application scenarios, the target cloud is detected for the open path influenced by the atmospheric conditions. Here, we perform an ammonia detection experiment under different humidity conditions.

Ammonia is released approximately 500 m from the spectrometer. The relative humidity (RH%) is measured with a hygrometer. Ammonia is vaporized by a sprayer without

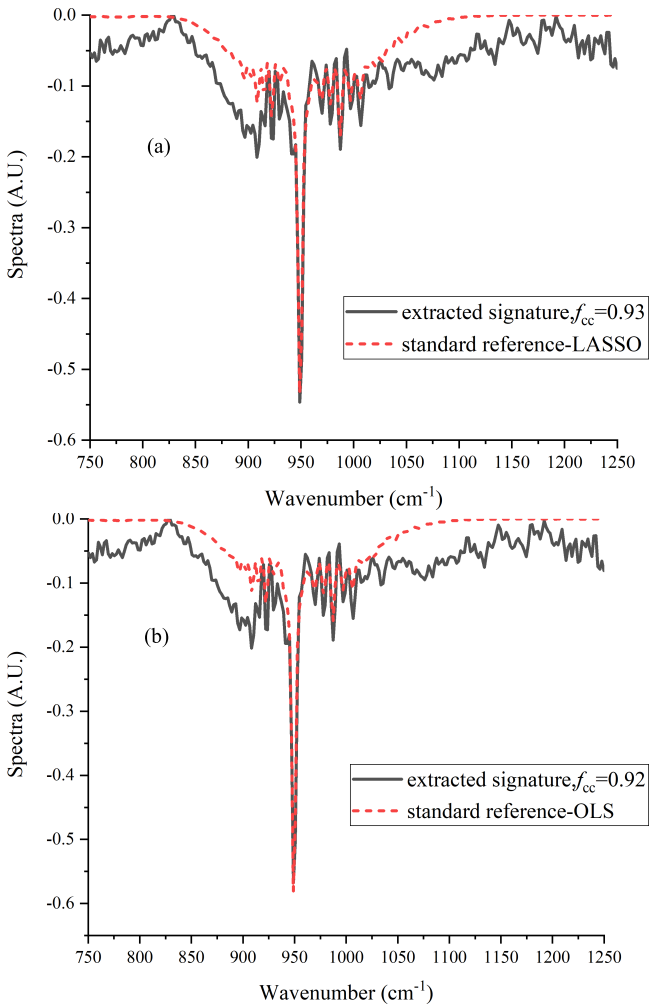

Fig. 19. Comparison of the extracted signature and identification results for the LASSO and OLS methods for the middle release case. All spectra are normalized and shifted for clarity. (a) Extracted signature and standard reference from the LASSO method, with $f_{cc} = 0.93$. (b) Extracted signature and standard reference from the OLS method, with $f_{cc} = 0.92$.

controlling the flow rate, and the concentrations are not strictly consistent for each experiment. Two typical RH% cases are chosen to show the influence of the atmosphere on background removal in remote sensing, as shown in Fig. 20. The high RH% is 60%–80%, and the low RH% is 40%–50%.

The transmittance spectra of ammonia are simulated for different CLs ranging from a very thin plume to a very thick cloud. A spectrum is used to represent a cluster of spectra with the f_{cc} values above 0.99, and five spectra are generated to represent different CL cases, as shown in Fig. 21(a).

The atmospheric spectra are simulated by MODTRAN, with scaled factors adjusted for the different humidity levels, as shown in Fig. 21(b). The scaled factors are set to six different values to represent typical RH% cases.

The baseline fitting uses wide Gaussian functions, which are 100 cm^{-1} uniformly distant and have a full-width at half-maximum of 200 cm^{-1}.

Under high-humidity conditions, water droplets hinder the transmittance of the target gas. The spectral features are very weak in the spectrum, and the water features in the

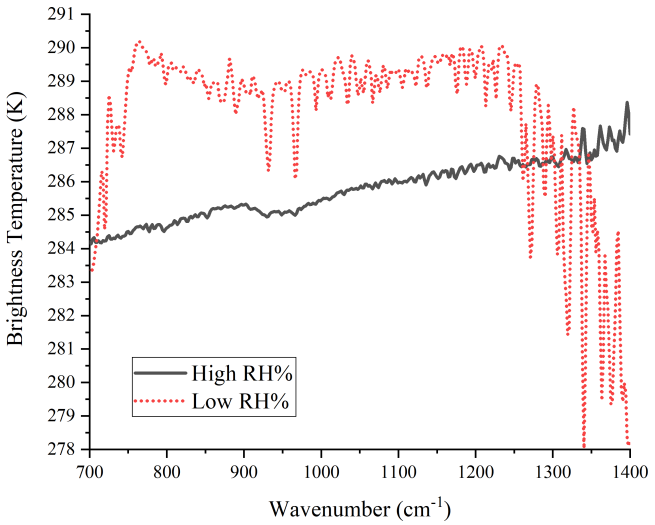

Fig. 20. Brightness temperature spectra of ammonia for the high RH% and low RH%.

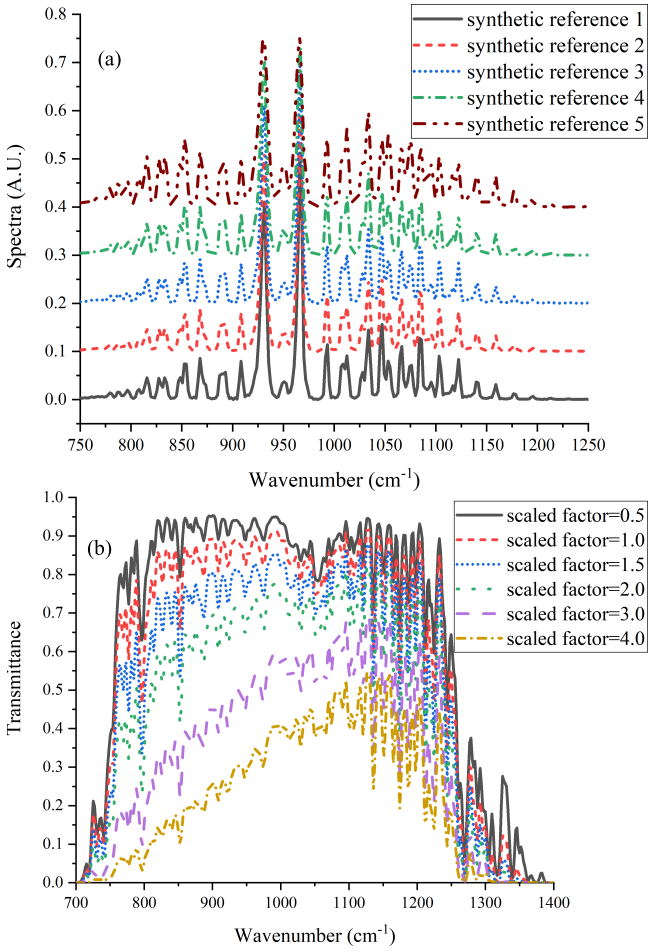

Fig. 21. Simulated ammonia references and atmospheric references. (a) Ammonia references for different CL values. (b) Atmospheric reference spectra for different RH% values based on MODTRAN, with scaled factors controlling the RH% value.

1250−1400 cm^{-1} band become emittance features. This is an extreme case for target detection because of terrible atmospheric conditions.

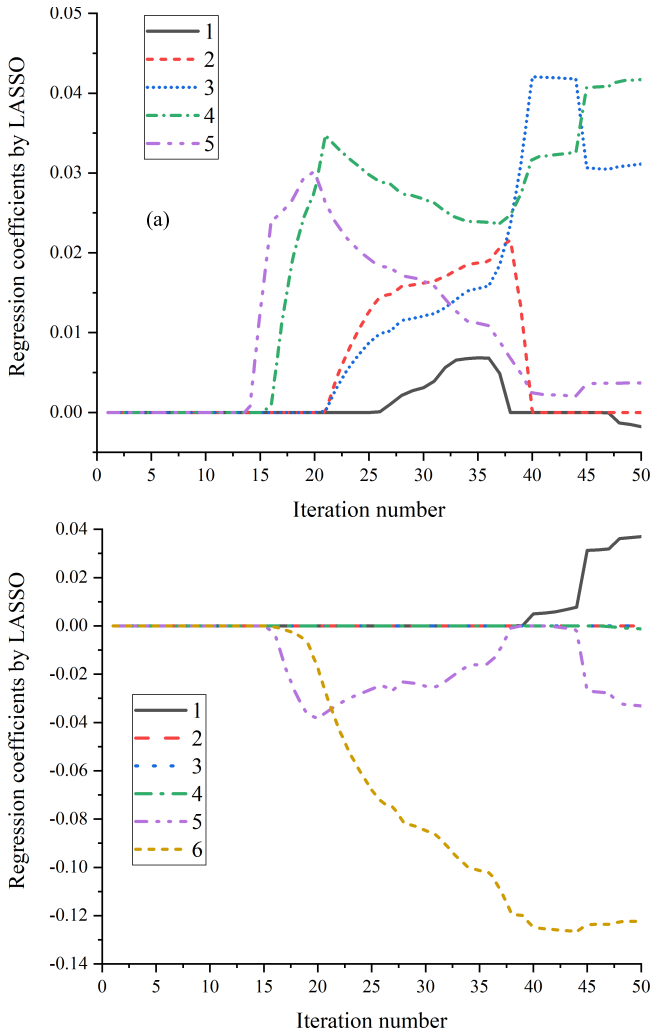

Fig. 22. Regression coefficients of the LASSO method for the high RH% case. (a) Regression coefficients of ammonia. (b) Regression coefficients of the atmosphere.

Using the LASSO method, the references of ammonia and the atmosphere are selected simultaneously. The LASSO regression is shown in Fig. 22. The fifth reference is selected as the ammonia standard reference in Fig. 21(a), and the fifth reference is selected as the atmosphere standard reference in Fig. 21(b).

A new reference matrix for LASSO is generated by combining the fifth reference in Fig. 21(a), the fifth reference in Fig. 21(b), and the original baseline fitting functions, and the measured spectrum is fit using this new reference matrix.

The OLS method uses the absorption coefficient of ammonia as the target reference and the first reference in Fig. 21(b) as the atmosphere reference because it lacks adaptivity and uses a fixed simulated atmospheric spectrum.

A comparison of the LASSO method and OLS method in the fitting of ammonia in the high-humidity case is shown in Fig. 23. The residuals for the LASSO method are slightly smaller than those for the OLS method.

The reconstructed background is shown in Fig. 24. There are some minor differences in the fitting spectra. The water

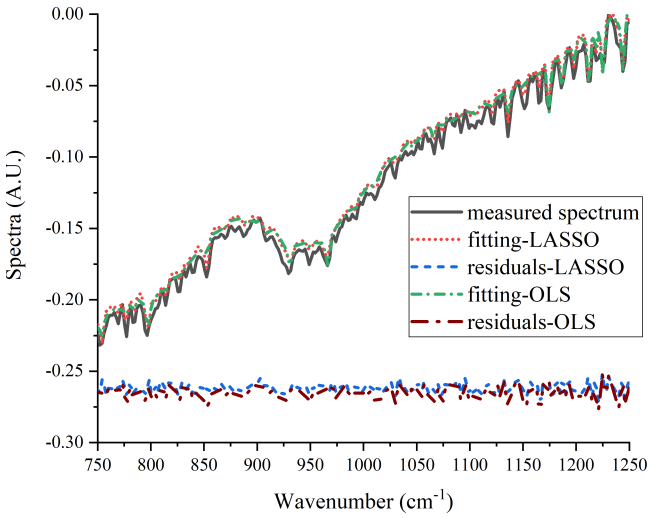

Fig. 23. Comparison of the LASSO method and the OLS method in fitting for ammonia in the high-humidity case. All spectra are normalized and shifted for clarity. The LASSO fitting uses the fifth reference as the target reference in Fig. 21(a) and the fifth reference as the atmosphere reference in Fig. 21(b), and the OLS method uses the absorption coefficient of ammonia as the target reference. The residuals are subtraction-fitted from the measured spectrum.

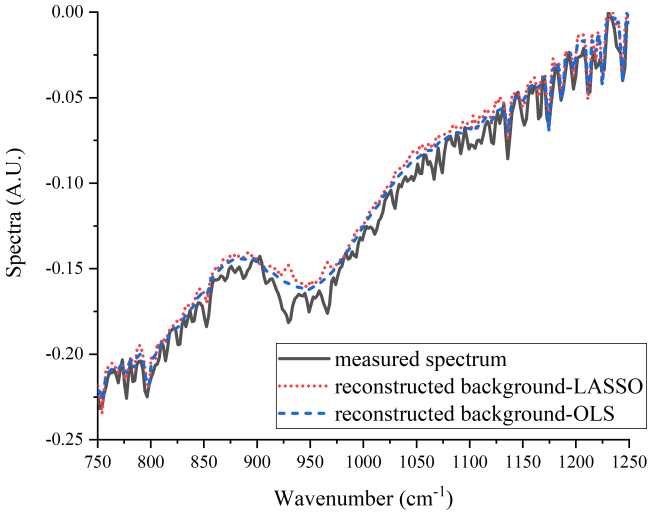

Fig. 24. Comparison of the backgrounds reconstructed by the two methods. All spectra are normalized and shifted for clarity.

absorption peaks at 850 and 1130 cm^{-1} are slightly better fit by the LASSO method than by the OLS method.

The extracted signatures and identifications are shown in Fig. 25. The extracted signatures are almost the same for these two methods, and the water interference peaks at 850 and 1130 cm^{-1} are slightly better subtracted by the LASSO method than by the OLS method.

The f_{cc} value of 0.67 for the LASSO method is slightly better than that for the OLS method. If the threshold is 0.65, the extracted signature of the LASSO method is identified as ammonia, whereas that of the OLS method is not. It should be noted that the threshold can be set for every target, respectively, and an appropriate adjustment could be used in threshold setting, although a good threshold requires data verification.

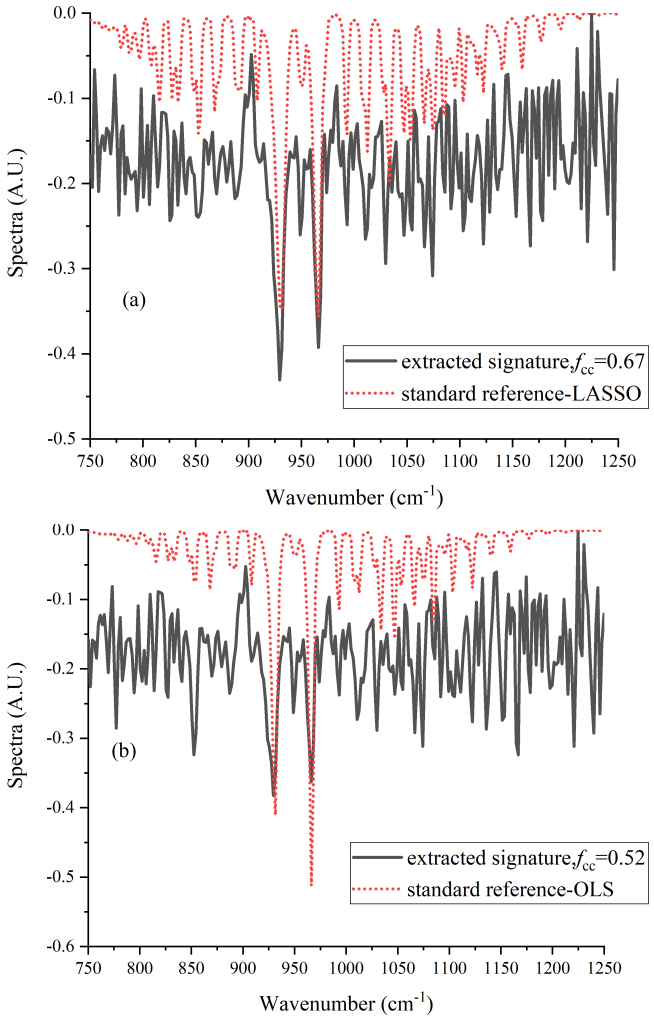

Fig. 25. Comparison of the extracted signatures and identification results for the LASSO and OLS methods for ammonia in the high-humidity case. All spectra are normalized and shifted for clarity. (a) Extracted signature and standard reference from the LASSO method, with $f_{cc} = 0.67$. (b) Extracted signature and standard reference from the OLS method, with $f_{cc} = 0.52$.

In the low-humidity case, the spectral features of the atmosphere and ammonia are obvious in Fig. 20. The LASSO regression is shown in Fig. 22. The fourth reference is selected as the ammonia standard reference in Fig. 26(a), and the first reference is selected as the atmospheric standard reference in Fig. 26(b).

A new reference matrix for LASSO is generated by combining the fourth reference in Fig. 21(a), the first reference in Fig. 21(b), and the original baseline fitting functions, and the measured spectrum is fit using this new reference matrix.

The OLS method uses the absorption coefficient of ammonia as the target reference and the first reference in Fig. 21(b) as the atmosphere reference. A comparison of the LASSO method and OLS method in the fitting of ammonia in the high-humidity case is shown in Fig. 27. The residuals for the LASSO method are almost the same as those for the OLS method.

The reconstructed backgrounds are almost the same, as shown in Fig. 28, and the extracted features are also almost the same, as shown in Fig. 29. However, the f_{cc} value

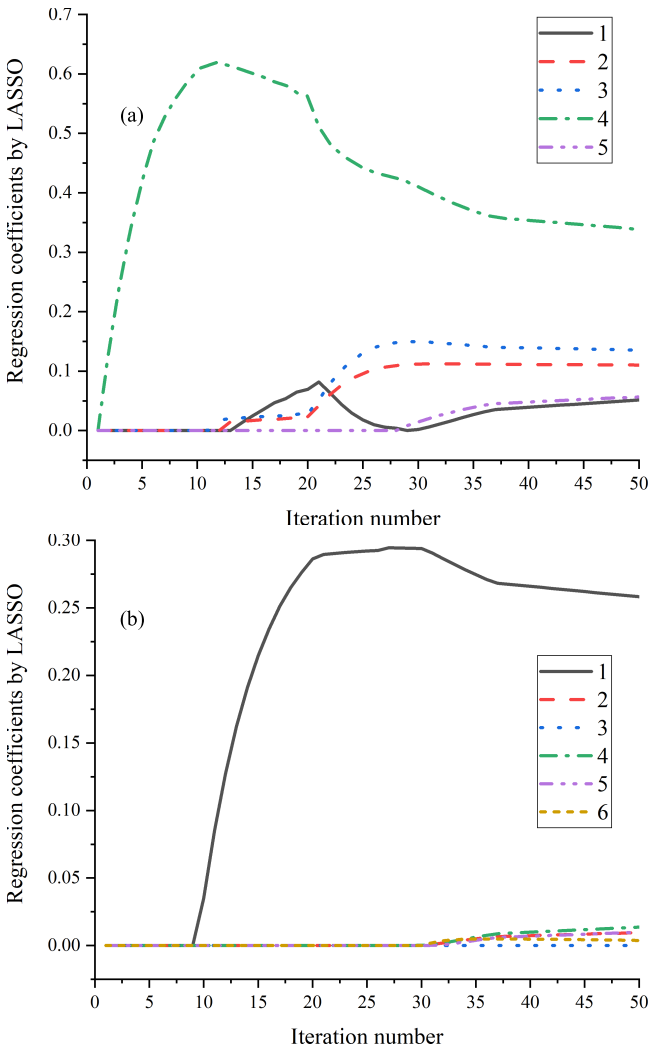

Fig. 26. Regression coefficients of the LASSO method for the low RH% case. (a) Regression coefficients of ammonia. (b) Regression coefficients of the atmosphere.

of 0.86 for LASSO is slightly better than that for the OLS method because a more approximate target reference is selected by LASSO.

From the ammonia detection experiment under different humidity levels, we find that compared with the OLS method, the LASSO method can adaptively reconstruct and remove the atmosphere, and better identification results are thus achieved.

C. Discussion

The method proposed in this article uses artificial reference data as well-defined variables, and this approach is very important in the LASSO method. Better references generally have small variable dimensions and provide efficient computations. Therefore, carefully choosing references can increase the computational efficiency.

Many algorithms have been developed to solve the LASSO problem, and the ADMM algorithm is just one of these methods. ADMM can use multiple cores to accelerate the computing process, leading to the reasonable selection of variables with satisfactory error levels. Other algorithms could yield the same results.

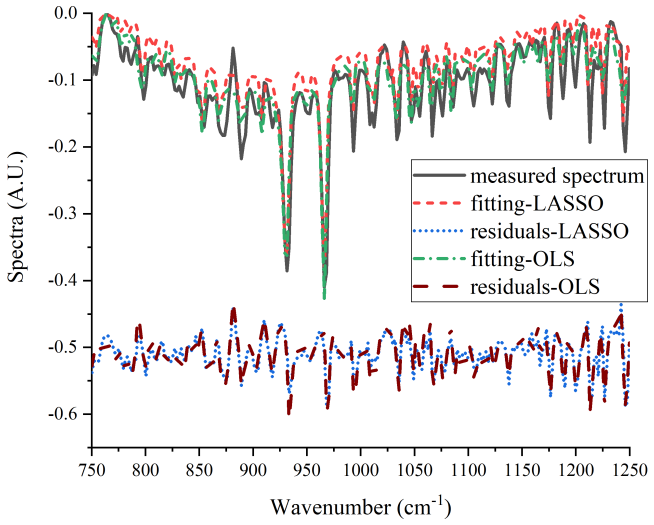

Fig. 27. Comparison of the LASSO method and the OLS method in the fitting of ammonia in the low-humidity case. All spectra are normalized and shifted for clarity. The LASSO fitting uses the fourth reference as the target reference in Fig. 21(a) and the first reference as the atmospheric reference in Fig. 21(b), and the OLS method uses the absorption coefficient of ammonia as the target reference and the first reference as the atmospheric reference in Fig. 21(b). The residuals are subtraction-fitted from the measured spectrum.

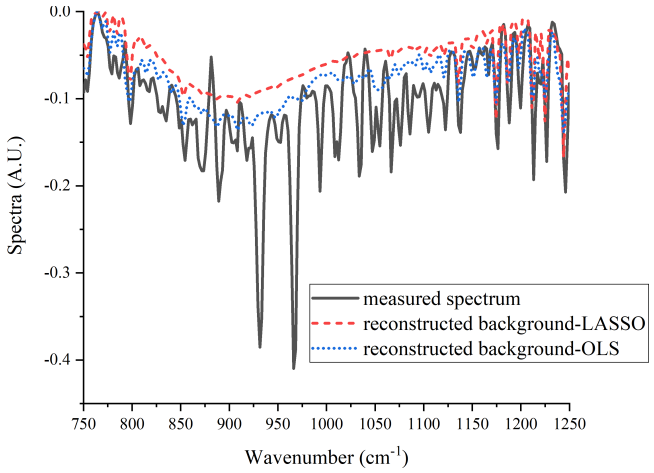

Fig. 28. Comparison of the backgrounds reconstructed by the two methods. All spectra are normalized and shifted for clarity.

A few factors, such as the concentration path length and atmospheric humidity level, are studied in this research. Beyond these factors, the temperature and pressure of the target cloud should be considered, for example, in explosive gas detection. The far-field atmosphere is also very complicated, and the spectral shape can be easily distorted by factors such as wind. The instrument used also has an implicit effect on the spectra. If all these factors are comprehensively included in the predefined reference spectra, fitting results with small residuals may be achieved.

A simple algorithm is described for synthetic reference spectra generation. A better selection result may be achieved if the synthetic references are more representative. A more reasonable stopping criterion and variable selection rule may improve the effect of feature extraction.

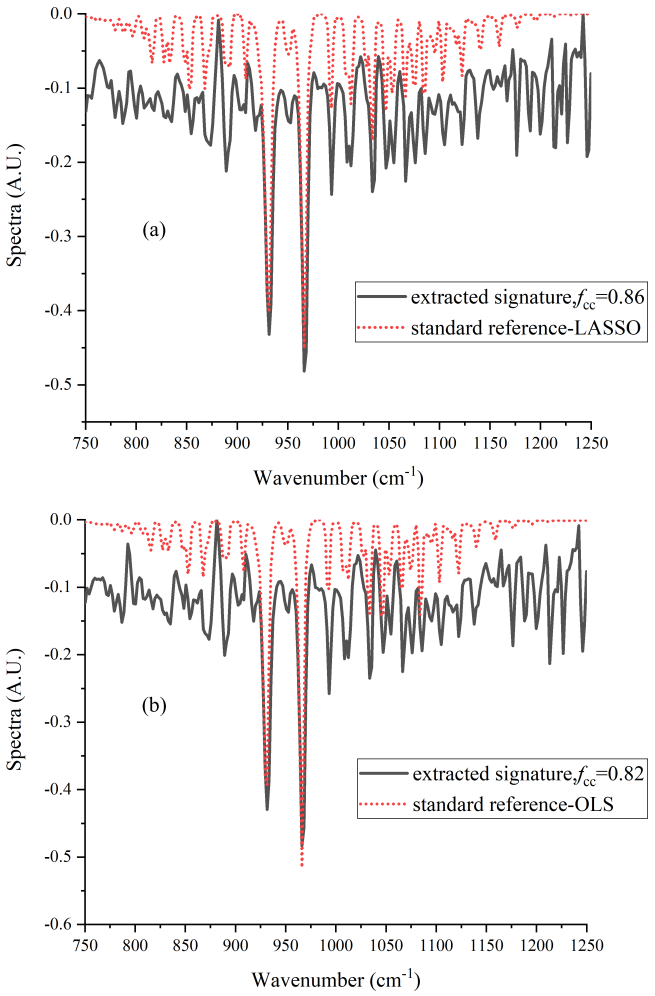

Fig. 29. Comparison of the extracted signatures and identification results for the LASSO and OLS methods for ammonia in the low-humidity case. All spectra are normalized and shifted for clarity. (a) Extracted signature and standard reference from the LASSO method, with $f_{cc} = 0.86$. (b) Extracted signature and standard reference from the OLS method, with $f_{cc} = 0.82$.

V. Conclusion

The brightness temperature spectrum is useful in hazardous cloud remote sensing. The spectrum is fitted using predefined references, including target and atmospheric references. The brightness temperature spectrum theory is valid when considering the thin-plume assumption, which restricts the application of the traditional methods in the thick-cloud cases. A modification has been made to effectively apply the brightness temperature spectrum theory for any thick-cloud case, and the measured spectrum is adaptively fitted by the LASSO method. With predefined references, the appropriate variable is selected by the ADMM algorithm, and the obtained fit spectrum is better than that from the OLS method with smaller residuals. Based on these steps, adaptive identification results are achieved by automatically selecting the most appropriate references. An indoor ethylene release experiment was performed to verify the method of selecting the best target spectrum, and an ammonia detection experiment with different humidity levels was performed to validate the adaptivity of the method under various atmospheric conditions.

With the "variable selection" merit of LASSO, the spectra of the target and atmosphere are adaptively selected based on the measured spectrum. This method can be used in many infrared signal processing areas. For example, a multiple gas mixture could be detected. In atmospheric inversion applications, the inversion error could be decreased by sacrificing some bias, and a good initial guess could be proposed by variable selection for fine optimization. This method could substitute the iterative optimization method for some applications.

A novel algorithm using LASSO is proposed for the remote sensing of hazardous clouds. Field experiments have proven the effect of this algorithm. This method may also be used in many other detection and inversion problems.

References

[1] D. Manolakis, "Signal processing algorithms for hyperspectral remote sensing of chemical plumes," in *Proc. IEEE Int. Conf. Acoust., Speech Signal Process.*, vols. 1–12, Mar./Apr. 2008, pp. 1857–1860.
[2] C. M. Charlton and B. Mizaikoff, "Sensing trace gases with quantum cascade lasers," *Photon. Spectra*, vol. 40, no. 4, p. 64, Apr. 2006.
[3] E. L. Holthoff and P. M. Pellegrino, "Photoacoustic spectroscopy for chemical detection," *Proc. SPIE*, vol. 8358, May 2012, Art. no. 83581I.
[4] D. M. Tratt *et al.*, "Airborne visualization and quantification of discrete methane sources in the environment," *Remote Sens. Environ.*, vol. 154, pp. 74–88, Nov. 2014.
[5] F. Bouffard and J.-M. Thériault, "Background contributions in direct and differential Fourier transform LWIR measurements: A comparative analysis," *Int. J. High Speed Electron. Syst.*, vol. 18, no. 2, pp. 263–276, Jun. 2008.
[6] J.-M. Theriault *et al.*, "CATSI EDM—A new sensor for the real-time passive stand-off detection and identification of chemicals," in *Proc. SPIE, Chem., Biol., Radiol., Nucl., Explosives*, vol. 7665, May 2010.
[7] R. Harig, P. Rusch, C. Dyer, A. Jones, R. Moseley, and B. Truscott, "Remote measurement of highly toxic vapors by scanning imaging Fourier-transform spectrometry" *Proc. SPIE*, vol. 5995, no. 10, 2005, Art. no. 599510.
[8] Q. Guo and G. W. Small, "Quantitative determination of methanol and ethanol with synthetic calibration spectra in passive Fourier transform infrared remote sensing measurements," *Appl. Spectrosc.*, vol. 67, no. 8, pp. 913–923, Aug. 2013.
[9] D. Manolakis and G. Shaw, "Detection algorithms for hyperspectral imaging applications," *IEEE Signal Process. Mag.*, vol. 19, no. 1, pp. 29–43, Jan. 2002.
[10] T. Burr and N. Hengartner, "Overview of physical models and statistical approaches for weak gaseous plume detection using passive infrared hyperspectral imagery," *Sensors*, vol. 6, no. 12, pp. 1721–1750, 2006.
[11] A. Beil, R. Daum, R. Harig, and G. Matz, "Remote sensing of atmospheric pollution by passive FTIR spectrometry," *Proc. SPIE*, vol. 3493, pp. 32–44, Dec. 1998.
[12] R. Harig and G. Matz, "Toxic cloud imaging by infrared spectrometry: A scanning FTIR system for identification and visualization," *Field Anal. Chem. Technol.*, vol. 5, nos. 1–2, pp. 75–91, 2001.
[13] C. M. Gittins, "Detection and characterization of chemical vapor fugitive emissions by nonlinear optimal estimation: Theory and simulation," *Appl. Opt.*, vol. 48, no. 23, pp. 4545–4561, Aug. 2009.
[14] R. Tibshirani, "Regression shrinkage and selection via the lasso: A retrospective," *J. Roy. Stat. Soc., B, Stat. Methodol.*, vol. 73, no. 3, pp. 273–282, Jun. 2011.
[15] H. Zou and T. Hastie, "Regularization and variable selection via the elastic net," *J. Roy. Stat. Soc., B, Stat. Methodol.*, vol. 67, no. 2, pp. 301–320, Apr. 2005.
[16] J. Li *et al.*, "Feature selection: A data perspective," *ACM Comput. Surv.*, vol. 50, no. 6, pp. 1–45, Jan. 2018.
[17] K. Sun, X. Geng, and L. Ji, "A new sparsity-based band selection method for target detection of hyperspectral image," *IEEE Geosci. Remote Sens. Lett.*, vol. 12, no. 2, pp. 329–333, Feb. 2015.
[18] B. B. Damodaran, N. Courty, and S. Lefevre, "Sparse Hilbert Schmidt independence criterion and surrogate-kernel-based feature selection for hyperspectral image classification," *IEEE Trans. Geosci. Remote Sens.*, vol. 55, no. 4, pp. 2385–2398, Apr. 2017.

[19] D. Yang and W. Bao, "Group lasso-based band selection for hyperspectral image classification," *IEEE Geosci. Remote Sens. Lett.*, vol. 14, no. 12, pp. 2438–2442, Dec. 2017.
[20] F. Santosa and W. W. Symes, "Linear inversion of band-limited reflection seismograms," *SIAM J. Sci. Stat. Comput.*, vol. 7, no. 4, pp. 1307–1330, Oct. 1986.
[21] R. Tibshirani, "Regression shrinkage and selection via the lasso," *J. Roy. Stat. Soc., B, Methodol.*, vol. 58, no. 1, pp. 267–288, Jan. 1996.
[22] P. Bühlmann and S. van de Geer, *Statistics for High-Dimensional Data: Methods, Theory and Applications*. Berlin, Germany: Springer, 2011, pp. 7–10.
[23] S. Boyd, N. Parikh, E. Chu, B. Peleato, and J. Eckstein, "Distributed optimization and statistical learning via the alternating direction method of multipliers," *Found. Trends Mach. Learn.*, vol. 3, no. 1, pp. 1–122, 2010.

Dacheng Li received the B.S. and M.S. degrees in mechanical engineering from the Hefei University of Technology, Hefei, China, in 2000 and 2014, respectively. He is pursuing the Ph.D. degree in optics with the University of Science and Technology of China, Hefei, China.

Since 2013, he has been with the Anhui Institute of Optics and Fine Mechanics, Hefei, China, where he is an Associate Professor with the Key Laboratory of Optical Calibration and Characterization. His research interests include optical system design, calibration, and signal processing in remote sensing applications.

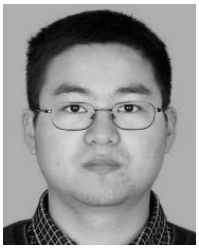

Fangxiao Cui received the B.S. degree in applied physics from Chongqing University, Chongqing, China, in 2008, and the M.S. and Ph.D. degrees from the University of the Chinese Academy of Sciences, Anhui Institute of Optics and Fine Mechanics, Hefei, China, in 2011 and 2015, respectively.

Since 2015, he has been with the Anhui Institute of Optics and Fine Mechanics, where he is an Assistant Researcher with the Key Laboratory of Optical Calibration and Characterization. His research interests include hyperspectral signal processing and pattern recognition.

Anjing Wang received the B.S. degree in computer science and technology from North China Electric Power University, Baoding, China, in 2007, and the Ph.D. degree in optics from the University of Science and Technology of China, Hefei, China, in 2017.

Since 2017, he has been with the Anhui Institute of Optics and Fine Mechanics, where he is an Assistant Researcher with the Key Laboratory of Optical Calibration and Characterization. His research interests include optical scene image simulation and infrared spectrum simulation.

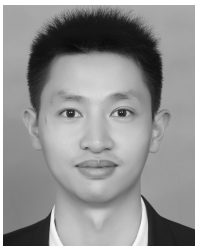

Yangyu Li received the B.S. degree in mechanical design and manufacturing and automation from Xidian University, Xi'an, China, in 2008, and the M.S. and Ph.D. degrees from the University of Chinese Academy of Sciences, Anhui Institute of Optics and Fine Mechanics, Hefei, China, in 2011 and 2015, respectively.

Since 2016, he has been with the Anhui Institute of Optics and Fine Mechanics, where he is an Assistant Researcher with the Key Laboratory of Optical Calibration and Characterization. His research interests include optical system design and calibration in remote sensing applications.

Jun Wu received the B.S. degree in cartography and geographic information system computer application technology from Northwest A&F University, Xianyang, China, in 2007, the M.S. degree from the University of Chinese Academy of Sciences, Hefei, China, in 2010, and the Ph.D. degree from the University of Science and Technology of China, Hefei, in 2013.

Since 2013, he has been with the Anhui Institute of Optics and Fine Mechanics, where he is an Associate Professor with the Key Laboratory of Optical Calibration and Characterization. His research interests include remote sensing signal processing, atmospheric radiation transmission modeling, and infrared scene simulation.

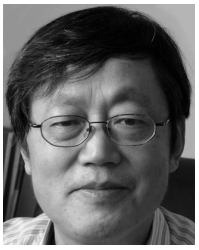

Yanli Qiao received the B.S. degree in computer communication from the Beijing University of Post and Telecommunication, Beijing, China, in 1982, and the M.S. degree in optics from the Anhui Institute of Optics and Fine Mechanics, Chinese Academy of Sciences, Hefei, China, in 1984.

He was a Visiting Scholar with the Institute of Physical Chemistry of Japan, Chiba University, Chiba, Japan, and also with the French National Institute for Agricultural Research (INRA), Paris, France. During his academic career, he served as the Team Leader and Department Director and is a Professor, the Ph.D. Supervisor, and the Deputy Director of the Anhui Institute of Optics and Fine Mechanics, where he is also the Chief Director of the Key Laboratory of Optical Calibration and Characterization, Chinese Academy of Sciences. Since 2011, he has been a Joint Professor with the University of Science and Technology of China. In 1994, he developed Chinese vicarious calibration techniques and took part in the construction of the Chinese Calibration Sites Technique System as the Chief Technique PI. He has been with the Anhui Institute of Optics and Fine Mechanics, Chinese Academy of Sciences, since 1984. He has been a pioneer in the development of optical polarimetric remote sensing techniques since 2002. He has been a Leading Scientist since 2006 in the development of remote sensing techniques for atmospheric components such as aerosol, carbon dioxide, water vapor, and methane based on airborne and spaceborne directional polarimetric sensing and hyperspectral detection. As the Chief Engineer, he was in charge of the development of the National Scientific Grand Infrastructure "Airborne Remote Sensing System for the Detection of Atmospheric Components" in 2010, with the goal of monitoring atmospheric aerosol, fine particles (PM10 and PM2.5), pollutants, and their column distributions. In 2011, he served as the Chief Administrator and was responsible for the fabrication of two spaceborne payloads, a directional polarimetric camera, and the monitoring of primary atmospheric greenhouse gases. These projects launched in 2017.

Mr. Qiao was a recipient of the Second Class Prize of the State Scientific and Technological Progress Award in 2012 and the First Class Prize of the Natural Science Award of Beijing City in 2012.